CHAPTER 3

DESIGN AND PIC SIMULATION OF MILO

3.1 Introduction

Simple, compact and efficient high power microwave sources are in demand for the recent upcoming applications, in electronic warfare and directed energy weaponary systems. Now-a-days efforts have been directed to develop HPM sources which do not require external DC magnetic field for the electron beam focusing, such as MILO, VIRCATOR and RELTRON. In the last decade, magnetically insulated line oscillator (MILO) has proven itself as an efficient crossed-field device to produce gigawatts of RF power. RF interaction structure of MILO comprises of the coaxial metal discs loaded periodic waveguide.MILO can be used as HPM source for ground based HPM weapon system and falls under the category of non-lethal weapon. This is able to operate in single shot as well as multiple shots with minimum peak power of 1GW in L to Ku-band frequency range. In order to explore this defense application based device, various authors reported different inherent properties of this HPM source. Mendel explored the concept of magnetic insulation in the coaxial transmission line in 1979 and 1983, using this concept various authors have made effort to invent high power RF oscillators that does not require external DC magnetic field. This idea, led to the invention of MILO. Further, [Lemke *et al.* (1997)] have reported improved experimental MILO device by employing an additional RF choke cavity in the upstream boundary to enhance the device efficiency. In 1995, Calico *et al.* have reported an experimental L-band MILO system producing 1.5 GW power at 1.2 GHz frequency. To improve pulse shortening observed by Calico *et al*., in an L-band MILO, Haworth *et al*. optimized cathode configuration in their device which yields 25% increase in the RF output power. For ensuring the magnetically insulated electron flow, they also replaced the constant radius cathode with taper cathode under the choke vanes during the experiment. They have reported 2.5 times longer pulse

length during RF power generation which helps to overcome the pulse shortening problem. Fan *et al.* has reported simulation study of improved MILO implementing the idea of Haworth *et al.* using KARAT code that generates peak power of 4.2 GW at the frequency of 1.76 GHz. This improved MILO has also been investigated experimentally after being optimized through simulation. Fan *et al*. used only one stub in their experimental MILO and their output has found to be unstable. In the present chapter, authors have reported stable RF output for defined pulse duration by placing four stubs 90^0 apart across the load side. Using PIC simulation code MAGIC, [Cousin *et al.* (2005)] reported simulation study on MILO. RF output power corresponding to the single mode can only be observed, using MAGIC code and it is impossible to observe the temporal signal growth of the other modes present in the device output, simultaneously. Here, work has been extended to study the MILO device performance for the RF output signal growth to other competiting modes alongwith the fundamental. This multimode analysis is essential to investigate the process of energy transfer from electrons to RF along individual mode that is not reported so far. A commercially available 3D PIC simulation code on 'CST Particle Suite' is used. In this chapter, an experimental device reported in the literature is typically selected for the multimode PIC simulation. The structure modeling is done considering design procedure of various structure parameters described in section II. We have improved the design procedure mentioned in ref. [Dwivedi and Jain (2013)] considering the effect of impedance to improve efficiency of the device. Further, eigenmode simulation of the device structure is performed to ascertain the operating mode, resonant frequency and electromagnetic fields configurations inside the RF interaction cavity. This electromagnetic simulation is carried out in absence of the electron beam which is also known as the cold analysis. The results obtained from the cold analysis

are used to predict the electron beam and RF wave interaction behavior of MILO device in the presence of the electron beam which is known to be as hot analysis. We have presented the device RF performance for the TM_{01} and TM_{02} modes in addition to the *TEM* mode during beam-wave interaction of the compact MILO. Percentage of the electromagnetic energy got transferred during beam-wave interaction in the different interacting modes for defined pulse duration also described here which was not explained earlier.

3.2 Device Design Procedure

Adequate designing of the HPM device helps to remove common shortcomings such as gap closure, beam interception, beam expansion etc.We have modified design procedure [Dwivedi and Jain (2013)] and consequently the expressionswhich were described by various authorswhile taking into account theimpedanceat input and output ends. For proper operation of RF interaction cavities we have selected TM_{01} operating mode. The RF cavity inner radius dimension was determined by device oscillation frequency using well known following formula:

$$r_d = \frac{c\, x_{m,n}}{2\pi f_r} \ . \tag{3.1}$$

where, c is velocity of light, f_r is resonant frequency of interaction structure; and $x_{m,n}$ is eigenvalue of the TM_{01} mode. Fundamental mode of MILO oscillation is π. At this mode each cavity behaves as a quarter-waveoscillator shifted in phase by πfrom its adjacent cavity. The outer radius (r_0) of different main cavities is determined using following relation:

$$r_0 = r_d + \lambda / 4 \tag{3.2}$$

During the process of beam-wave interaction, to prevent propagation of reflected wave towards choke radius it is necessary to design the choke properly. Choke cavity act as an in-phase reflector or low pass filter because its inner radius is kept at high cut-off frequency than the cut-off frequency of SWS inner cavityradius. Choke cavity radius is calculated using flow impedance parameter. Flow impedance (Z_f) also help in decided the impedance of pulse forming line (towards input before tapered cathode) [Mendel *et al.* (1992)],

$$Z_f = r_{a1} - r_c \,. \tag{3.3}$$

where r_{a1} represents choke radius and r_c represents radius of cathode. In addition, to this inside the device, there must be the impedance difference between the last choke disc and the first primary disc. At lower impedance there is more current in the electron flow, and therefore, more power available for microwave generation. Using flow impedance the effective distance between radius of cathode and choke cavityis measured. Expression for flow impedance is written as,

$$Z_f = \frac{V}{\sqrt{I_a^2 - I_c^2}} \,. \tag{3.4}$$

Difference between anode (I_a) and cathode current (I_c) is known as the leakage current caused due to the space charge effect. Anode and cathode currents are defined in previous chapter. Improved MILO has a tapered cathode shank in the choke vane region while the compact MILO has a constant radius cathode over the entire length of the tube. Changing to the tapered shank in the choke region tends to increase RF output power while tripling the pulse duration [Haworth *et. al* (2000)]. The optimum length of taper (l) can be expressed considering operating mode using relation:

$k_z l = \pi$; here, $k_z = 2\pi / \lambda$, thus, $l = \lambda / 2$.

Top radius of taper (r_1) = $0.3\lambda/\pi$and launch point radius (r_2) = $0.8\lambda/\pi$ (3.5)

It is so chosen to have in phase reflection and to prevent propagation of reflected wave. Tapering at the input side of the cathode provides gradual decrease in impedance, as r_c increases. On tapering it, linear variation in impedance causes performance improvement of the device due to the pulse lengthening.

The extractor part includes last MILO vane (called extractor vane) and the axial distance from the extractor vane and the coaxial transmission line forms extractor gap). The inner radius of the extractor vane is slightly larger than the rest of the vanes to provide a good match of the extractor gap electric field to that of the output coaxial transmission line (CTL). Main function of extractor cavity is to convert standing wave into the travelling wave which is to be transported outside. Radius of extractor cavity is same as outer radius of beam dump, but larger than interaction cavities, since the radial component of RF electric field is maximum on the inner radius of extractor vane. This amount of radial component on vane tip is coupled directly to the output coaxial transmission line [Dwivedi and Jain (2013)].Thus to extract RF energy it is necessary to couple the extractor cavity with the output waveguide. The covering of collector on cathode constitutes an additional cavity which plays an important role in storing the RF energy generated in MILO, and then transfers this energy to the external load in the form of pulse, thus load impedance is written as,

$$Z_0 = 60 \ln(r_{a3} / r_c) . \tag{3.6}$$

where, r_{a3} represents extractor radius and r_c represents radius of cathode.

Periodicity between discs plays an important role during beam-wave interaction mechanism. During operation of MILO, both electric and magnetic fields arise from the DC pulsed power source and their ratio is a weak function of voltage. The axial drift velocity v_d of electrons is expressed as:

$$\frac{v_d}{c} = \frac{Z_p}{Z_0}. \tag{3.7}$$

where, $Z_p\,(=23/\ln(r_{a1}/r_c))$ represents impedance of the magnetically insulated sheath.MILO operates at a constant drift velocity and it does not require tuning between operating voltage and magnetic field as in case of the magnetron. This condition occurs because the drift velocity is proportional to impedance, which is independent of the applied voltage. During operation of the device, the self magnetic field automatically adjusts to the changing drive voltage maintaining the constant drift velocity.

Drift velocity of electron beam = Phase velocity of RF (3.8)

$$v_p = \omega/\beta = 2Lf \tag{3.9}$$

In Equation (3.9), v_p, L and f represent the phase velocity, the disc periodicity and oscillation frequency, respectively. Drift velocity (v_d) is calculated using Equation (3.7). Referring (3.7) periodicity between discs can be calculated, on substituting drift velocity equals to the phase velocity. Equation (3.8) also represents synchronism condition, ensures energy exchange between RF waves and electron beam, thus RF emission become possible. Distance between extractor vane and beam dump also depend on the periodicity. The spatially averaged current between RF cavity [Lemke *et al.* (1997)] and the cathode is expressed as follows:

$$I_{av}(t) = I_s \frac{\sin(\theta/2)}{\theta/2}\sin\omega t\ . \tag{3.10}$$

where, I_s represents amplitude of modulated current known as spoke current, which is responsible for storing energy inside the RF cavities.The potential difference $V(t)$ between the cavity and the cathode, induced by electromagnetic wave is$V_0 \sin \omega t$. During beam-wave interaction RF voltage must be greater than DC beam voltage.

Hence, the average power flow during beam-wave interaction from electron beam to field can be written as:

$$P_{RF} = \frac{1}{T}\int_0^T I_{av}(t)V(t)\,dt\,. \tag{3.11}$$

Substituting the expressions for I_{av} (t) and V(t) from the above in the Equation (3.11), average power generated is expressed as [Lemke et al. (1997)]:

$$P_{RF} = \frac{1}{2}\frac{Sin(\theta/2)}{(\theta/2)} I_s V_0. \tag{3.12}$$

Because a spoke takes approximately one-half cycle to cross the AK gap, its transit angle (θ) is π. Hence, relation (3.12) is expressed as $P_{\mathrm{RF}} = 0.32 I_s V_0$.As spokes electrons traverses the anode cathode gap, their energy gets converted into RF energy with efficiency known as conversion efficiency. The conversion efficiency (relative to the input power) can be given as:

$$\eta_{elec} = \frac{P_{\mathrm{RF}}}{V_0 I_a} = 0.32(1-\frac{I_{cr}}{I_a}) \quad . \tag{3.13}$$

Extraction efficiency is the product of conversion efficiency and total efficiency in MILO. The load region of MILO comprises of the part of cathode inside the collector (Load-Length) and the remaining cover part is named as collector cavity depth. For magnetic insulation to takes place in MILO, load part plays an important role. During the operation, electron current flow through load side generates the required magnetic field which ultimately helps in insulating the electron flow in the SWS region. Current at which magnetic insulation takes place is known as the critical current (see Figure 3.1). Expression for calculating length of the cathode under collector has already been defined in literature. Load length is also responsible for energy extraction. The additional cavity which is at the load side works as thecapacitor. This capacitor isused to extract out RF energy from the collector as well as SWS. As $C = \varepsilon_0 A / d$, where d is

the axial depth of collector cavity and as its value increases then capacitance 'C' decreases and vice-versa. Axial depth (d) between the cathode and collector cavity is determined using relation:

$$f = \frac{4.77}{d}\ln(\gamma_0 + \sqrt{\gamma_0^2 - 1})\ \text{GHz}\ . \qquad (3.14)$$

In above equation, d is in cms. In improved MILO this axial depth is referred as load length. Depending on operating frequency load length (d) is calculated. This load length is inversely proportional to the RF output power generated from device [Lemke *et al.* (1997)].As can be seen from Figure 3.2, that two stubs are placed at $\lambda_g/4$ distance from the extractor cavity for impedance matching. The stubs should be placed symmetrically for the stable device operation and maximum power transfer. Length of collector is determined using relation [Dwivedi*et al.* (2013); Cousin *et al.*(2005)]:

$$I_{charging} = I_0(\mathrm{L}_c / \mathrm{r}_c)\frac{[\sqrt{\gamma_0} - 0.847]^2}{[\ln(\mathrm{r}_a / r_c)]^2}$$

where, L_c is the length of collector.

If the cathode-collector part is long enough, as in conventional MILO[Dwivedi*et al.* (2013), R. Cousin (2005)]then it is difficult to extract energy stored in cavity. This will be responsible for the poor inefficiency in conventional MILO since electrons accumulated their does not take part in beam-wave interaction process. In improved MILO, the length that the cathode extends into the beam dump is 5mm. Thus the load current or critical current which is required for magnetic insulation is generated from the side and the end surface of cathode extended into the beam dump region. This also helps in enhancing feedback.

Design of improved MILO structure reduces overall length of the MILO which is due to the fact that a large fraction of the dc input current is utilized to form the load current.Considering the above designing procedure, relevant device parameters described in section IV, can be validated. We have reported the whole design procedure for the first time.

3.3 Introduction to PIC Simulation

3.3.1 Structure modeling

A typical experimental compact MILO device reported in the literature has been selected for the PIC simulation investigated in the present study [Fan *et al.* (2007)]. In this section considering the relevant device parameters (described in Table 1), electromagnetic simulation study in the electron beam absent (cold condition) as well as the PIC simulation study for the electron beam and RF wave interaction (hot condition) study has been described. Simulation study is carried out using a commercially available PIC simulation code, 'CST Studio Suite'. Selection of high power microwave source MILO, depends upon both structural parameters(cathode radius, discs hole inner radius, periodicity between discs, inner radius of collector and length of cathode over collector) and beam parameters (such as beam voltage, beam current, pulse width and pulse rise time). These variousparameters effects overall device efficiency, released RF energy and RF power output.

3.3.2 RF interaction cavities simulation (beam absent condition)

To explore the electromagnetic behavior of the RF interaction region of the MILO structure in the absence of the electron beam (cold condition) eigenmodeanalysis is carried out. For simulation, the device structure has been modeled using typical

parameters of the selected compact MILO.Using design specifications defined in Table 1, structure modeled for performing simulation is shown in Figure 3.1.

Table 3.1. Design specifications for Improved MILO [Fan *et.al* (2007)].

Particulars	**Specifications**
Voltage	600kV
Current	52kA
Cathode Radius (r_c)	28 mm
Anode Radius (r_a)	85 mm
SWS Vane Radius	45 mm
Extractor Vane Radius	54 mm
Choke Vane Radius	42 mm
Vane Thickness (T)	4 mm
Periodicity (L)	19 mm
Beam dump outer Radius	54 mm
Beam dump inner radius	54 mm

Beam absent analysis is performed using CST Microwave studio to ensure the excited mode, resonant frequency and electromagnetic fields configurations inside the cavity. Eigenmode simulation analysis is carried out to identify the presence of the electromagnetic mode inside the interaction cavities. This is confirmed by observing the RF electric and magnetic fields pattern. This is essential and first step of demonstrating suitable mode for carrying out beam present simulation. In order to analyze the structure using simulation code various boundary conditions need to be satisfied to provide solutions of problems in a region of finite dimensions. Structure to be modeled operates like a perfect electric conductor, i.e., all tangential electric field are set to be zero. Discs are made of perfectly conducting material and its background material is kept normal (vacuum).

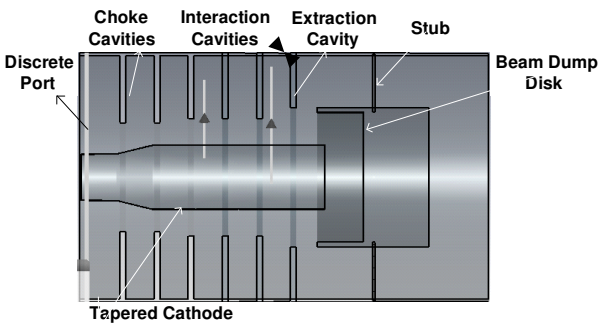

Figure 3.1: Improved MILO structure modeled using simulation.

In order to solve electric and magnetic profiles using Maxwell's equations, simulation code uses the finite integration method which requires computational domain to be covered by hexahedral mesh. Number of mesh lines per wavelength is also an important parameter and is connected to the wavelength of the highest frequency in simulation.It defines the minimum number of mesh lines in each coordinate direction that are used for a distance equal to this wavelength.

The space between two consecutive discs forms an RF cavity. Figure 3.2, represents a typical conventional MILO consisting of seven vanes forming six cavities.Two cavities are formed towards the pulsed source left side of Figure 3.2a and Figure 3.2b named as RF choke cavities. These cavities are employed to enhance feedback in RF interaction cavities. Thus cavitycontribute in the growth of RF waves. Thus,choke cavity section acts as an in-phase reflector and this operation is being confirmed by absence of electric field in choke cavity. Figure 3.2a and Figure 3.2b represents π mode operation along SWS confirm properly TM_{01} mode operation along RF circuit. Figure 3.2c and Figure 3.2d represents contour plot and arrow representation conforming desired mode operation along RF interaction cavity. Figure 3.2e represents dispersion diagram for MILO in absence of the electron beam for TM_{01} mode of operation which helps further for calculating the phase velocity.

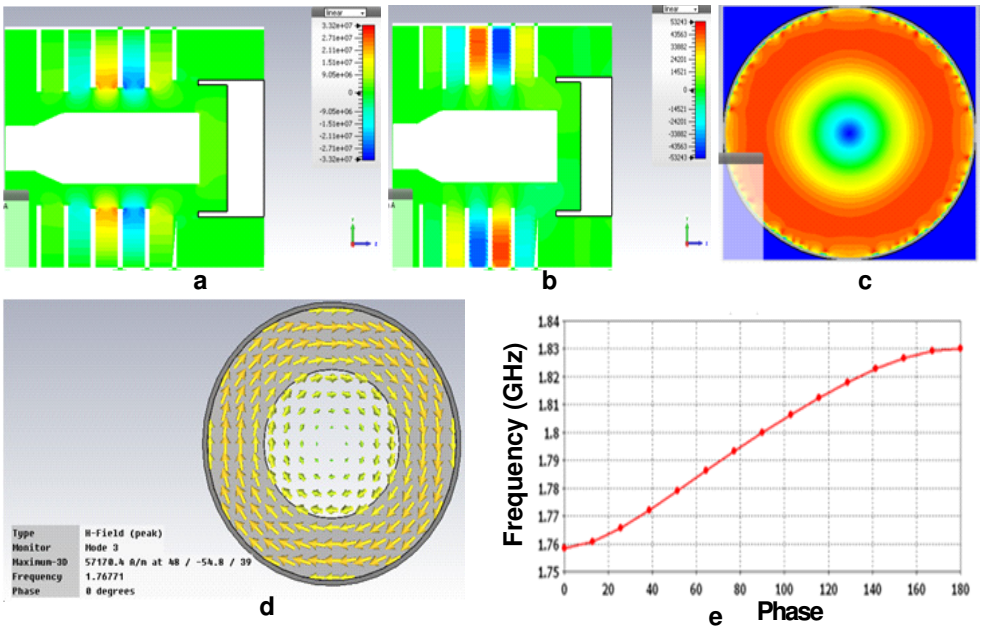

Figure 3.2: **(a)** 2D view of electric field variation along the SWS cavities (π mode operation), **(b)** Magnetic field variation along SWS cavities, **(c)** 3D contour plot conforming TM_{01} mode operation, **(d)** Arrow representation, **(e)** dispersion diagram for desired operating mode.

3.3.3 PIC simulation of the MILO structure (beam present condition) —beam-wave interaction

To investigate the electron beam and RF wave interaction behavior and RF signal growth in the device, 3D PIC simulation is performed in presence of the electrons, reconfiguring the commercially available universal PIC code "CST particle studio". It is graphic user interface (GUI) based 3D simulation code and persists various features such as PIC phase space monitor, PIC-2D monitor and its post-processing module. A waveguide port is defined at the output section to determine the temporal RF output power developed at respective modes.The temporal evolution of the electron beam inside the electromagnetic structure of the MILO device is investigated by subjecting cathode an intense electric field.As per the beam

parameter of the selected MILO device, DC pulse voltage of rise time = 30ns, 20ns flat top, 35ns fall time is applied. During PIC simulation, DC pulse voltage is injected from left boundary using discrete port shown in Figure 3.1. Discrete port works as a voltage source of constant amplitude during beam present simulation. Excited pulse signal generates negative potential at the surface of cathode. DC voltage of 600 kV is developed for defined rise time of 30 ns. At this rise time beam-wave interaction mechanisms starts inside the electromagnetic structure.

3.4 Results and Discussion

Magnetically insulated line oscillator (MILO) is a high power oscillator in the microwave frequency range where DC electron beam energy is converted into RF energy and it does not require additional DC magnetic field for the focusing of the electrons.The designed device is PIC simulated, as per procedure described in above section to study the electron beam and RF wave interaction mechanism inside the MILO device which results into the growth of RF signal. The observations and results of the PIC simulation are discussed below.

3.4.1 Energy exchange between electrons and RF field

To get the information about perturbation of the particles in terms of energy / phase and bunching phenomena, particles are monitored in 2D planes during simulation. This monitoring is done at regular time interval during the simulation to understand the energy exchange between the electrons and RF field. When electrons at the cathode surface acquire sufficient energy, highly intense electric fieldis generated. Due to this amount of electric field, electrons are accelerated due to the potential difference developed between cathode and anode (as shown in Figure 3.3a. During simulation, three phase of operation are observed in MILO [Lemke (1997)].

These phases are defined as pre-oscillation phase, linear phase and third are named as non-linear phase of operation. Pre-oscillation phase can be observed from Figure3.3a. During this phase of operation only radial component of electric field intervenes, that corresponds to the starting of the electron emission as in Figure 3.3a. As can be seen from Figure3.3b, the load current is insufficient to generate the magnetic field required to insulate the electron flow in the SWS region [Lemke *et al.* (1997)]. During this phase there is no excitation of resonant waves. Magnetically insulated sheath is formed between tip of discs and cathode during second phase of operation named as linear phase of operation and can be observed from Figures 3.3(c-e). Electrons get drift parallel to cathode due to generation of minimum load current produced by setting the length of emitting cathode beyond the extractor gap that also contributes in optimizing the feedback. For maximum transfer of energy from beam electrons to the modes of the periodic resonator, the emitted current under the collector should be equal to the minimum current needed to insulate the electron flow.

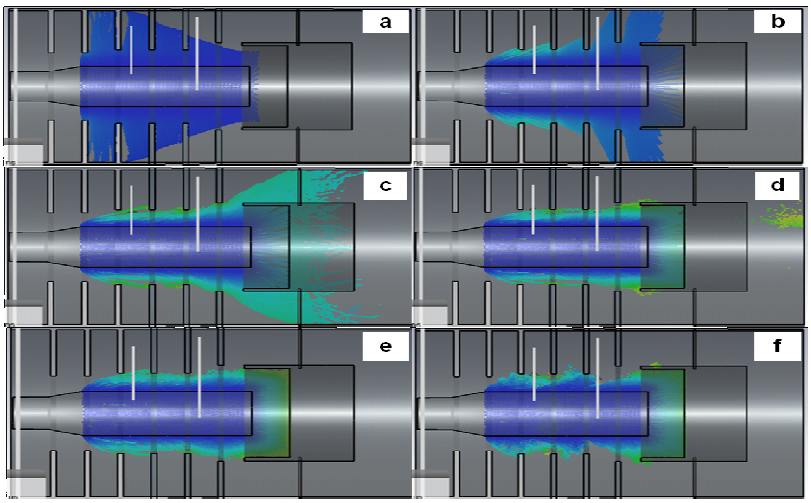

Figure 3.3: Linear phase of operation.

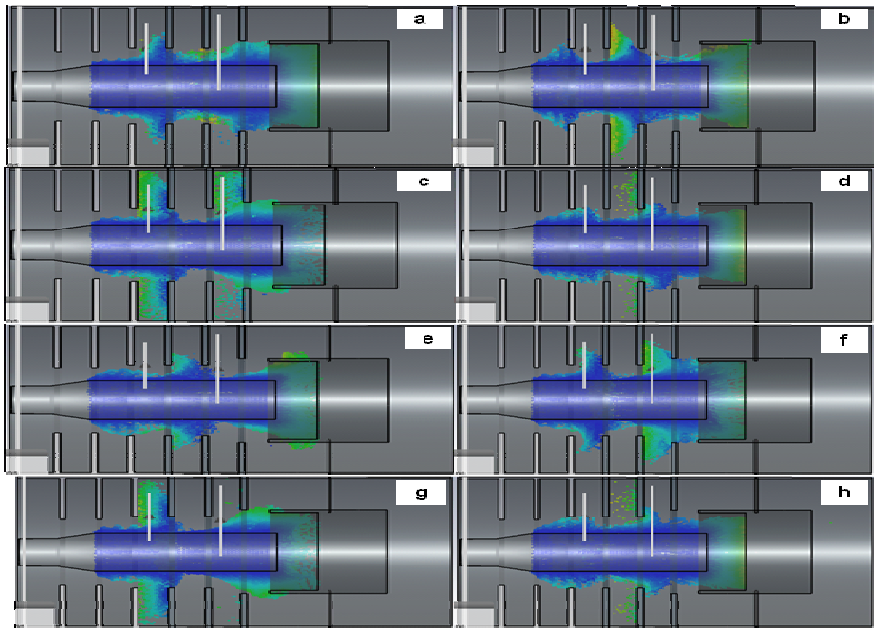

Figure 3.4: Non-Linear phase of operation.

Third phase of operation can be observed clearly from Figure 3.4, that corresponds to the nonlinear phase of operation in MILO. During this phase, beam-wave interaction process occurs. Drift velocity of beam electrons along the magnetically insulated sheath get modified due to presence of axial and radial component of electric field along the magnetically insulated electron sheath. Thus electrons of the same layer get accelerated or decelerated, generates instability known as Diocotron instability as can be seen from Figure 3.4a, and Figure 3.4b. Radial component of the electric field is responsible for spoke formation and energy transfer occurs in the structure due to axial component of the electric field. Due to relativistic Brillouin flow, transient state allows the establishment of the RF waves in the SWS structure and oscillation starts inside the periodic resonator instable TM mode. For efficient beam-wave interaction in MILO, slow space charge waves must be synchronized with the drift velocity of electron beam as described in above section. When electron spoke acquire kinetic energy equal to gap voltage they cross the anode-cathode gap shown in Figures 3.4c-

e. Under Diocotron instability, few electrons migrates towards anode in bunch form, that is called spokes, characterizing a leakage current or RF current resulting from the interaction in SWS. In transiting the anode-cathode gap, the RF current or leakage current interacts with a modulated anode cathode gap voltage thereby generating microwaves. When the geometry of structure ensures synchronism between the electron drift velocity and the phase velocity of desired mode, energy exchange takes place between RF wave and electron beam, thus RF emission becomes possible.

It can be observed from above snapshots taken during simulation that a spoke is on for a half-cycle of the oscillation and off for the remainder of the cycle, similar to a train of step functions. Because a spoke takes approximately one-half cycle to cross the anode-cathode gap, its transit angle is π.As spokes electrons traverses the anode cathode gap, their energy gets converted into RF energy with some efficiency known as electronic efficiency. RF emission becomes possible, when synchronism between the velocity of drift electron and the phase velocity of RF wave occurs, then only energy exchange takes place.

3.4.2 RF output power and efficiency

In order to observe RF output power at *TEM* mode, waveguide port is implemented at output coaxial transmission line. The load section and waveguide forms coaxial transmission line that helps in transmitting developed RF to transmit outside.For predicting RF signal growth and energy at respective mode, commercial PIC simulation code 'Particle Studio" has proven to be a useful tool for multimode beam-wave analysis. In order to observe temporal RF output power at TM_{01} mode, waveguide port can be shifted by extending circular waveguide.In order to maximize and stabilize the RF output power, launch region consists of choke cavity that helps

in reflecting backward wave in phase with the forward wave thus acts as an in-phase reflector. Figure 3.5,show the temporal RF output power developed in *TEM* mode which begins to grow at 30 ns and maximum power 4.5 GW is developed for desired pulse duration that confirms the stable operation at desired mode.

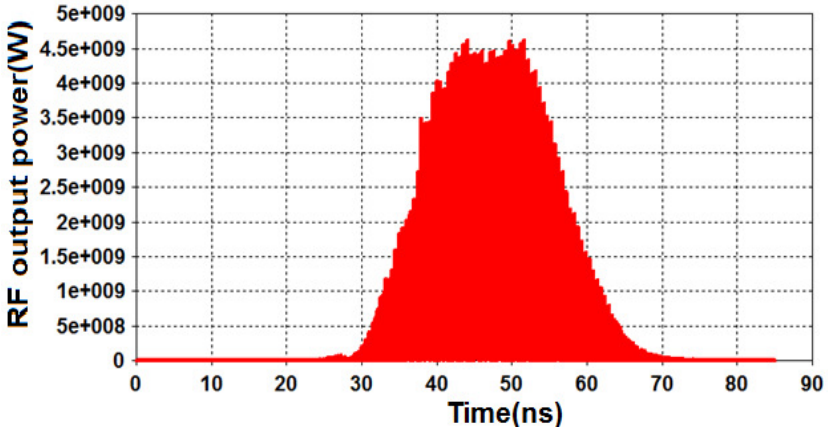

Figure 3.5: Temporal RF output power at *TEM* mode.

During simulation stubs are placed at λg/4 distance for better impedance matching or maximum power transfer. Stub provides mechanical support to collector and also at a distance $\lambda_g/4$ it works as open circuit stub. This phenomenon provides us to radiate TM wave with minimum losses due to reflection through stub. Since the stub acts like a DC short and RF open so there by increase in the amount of feedback of load current. The authors placed four identical stubs at 90^0 apart. Due to proper stub matching, stable RF output power is developed at desired mode.

Fourier transform of RF signal amplitude developed at waveguide port corresponds to operating frequency at which structure resonates. A peak is observed at 1.76 GHz at which structure resonates observed from Figure 3.6. It can be seen from figures that the peak amplitude of second harmonic is less than the fundamental.

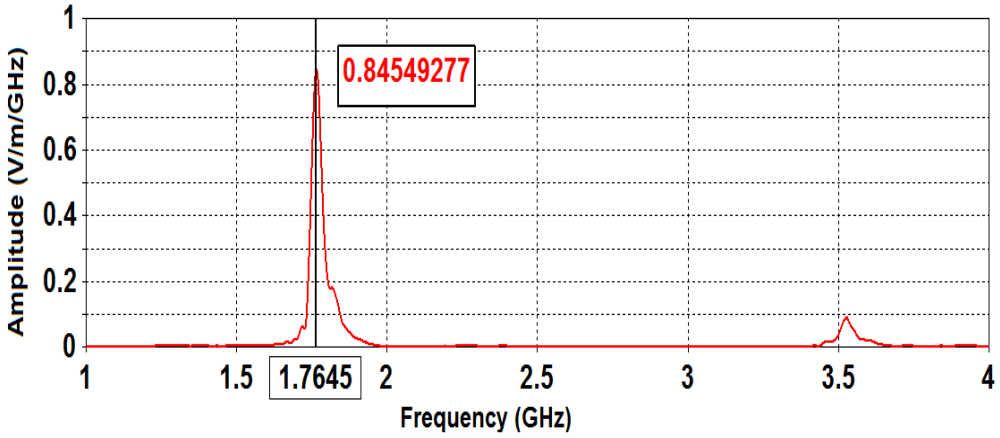

Figure 3.6: Frequency spectrum at *TEM* mode.

Comparison of RF output powers considering one stub and two stubs is shown in Figure 3.7, obtains using PIC simulation code. It can be seen that simulation results obtained using CST-Particle Studio suite agreed well with that of simulation code used by Fan *et al*. and effect of implement two stubs at output also helps in maximum stable RF output power transfer. Both developed power are found in good agreement.

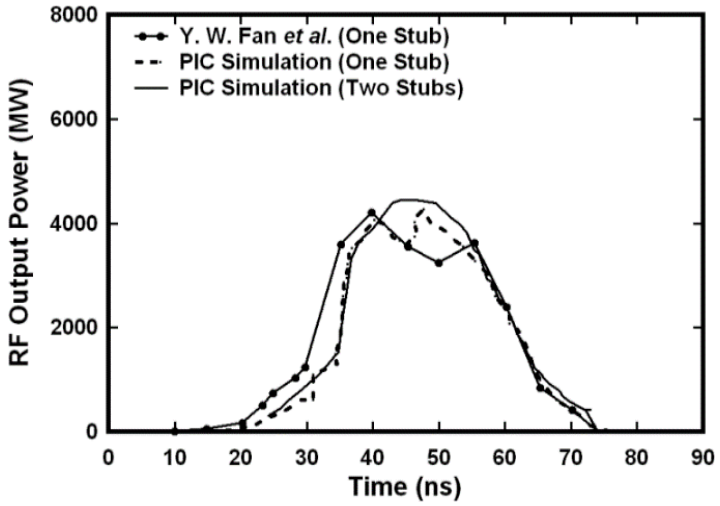

Figure 3.7: RF output power comparison.

To observe the RF output power at TM_{01} mode, which corresponds to oscillating mode of MILO, power should be extracted through coaxial waveguide as shown in Figure 3.8a.

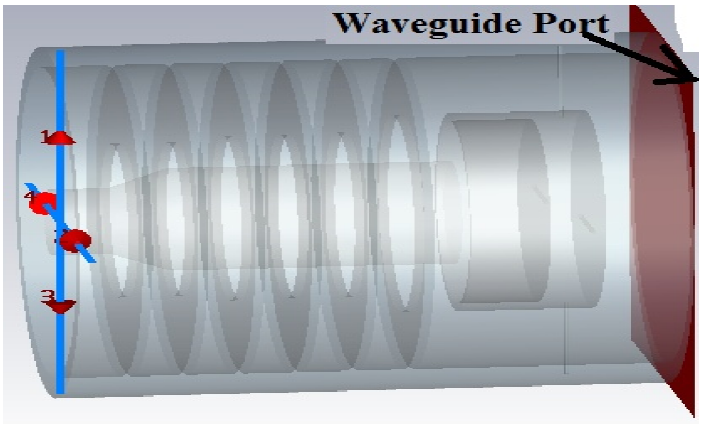

(a)

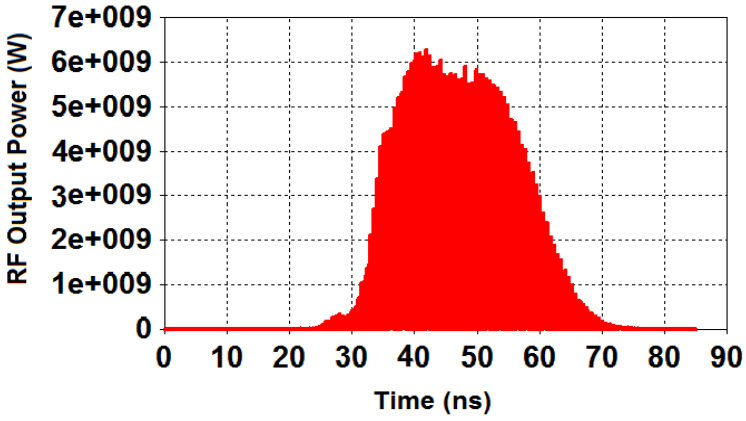

(b)

Figure 3.8: (a) Improved MILO structure for extracting power in TM_{01} mode**, (b)** Temporal RF output power developed at TM_{01} mode.

It can be concluded from Figure 3.8b that RF output power developed at TM_{01} mode is greater than RF output power at TEM mode with the same resonating frequency. On taking the fourier transform of signal amplitude developed at TM_{01} mode, observed highest peak is at 1.76 GHz, which confirms the frequency of operation of the device as shown in Figure 3.9. The second peak is obtained at 3.5GHz, which correspond to its second harmonic i.e TM_{02} mode.

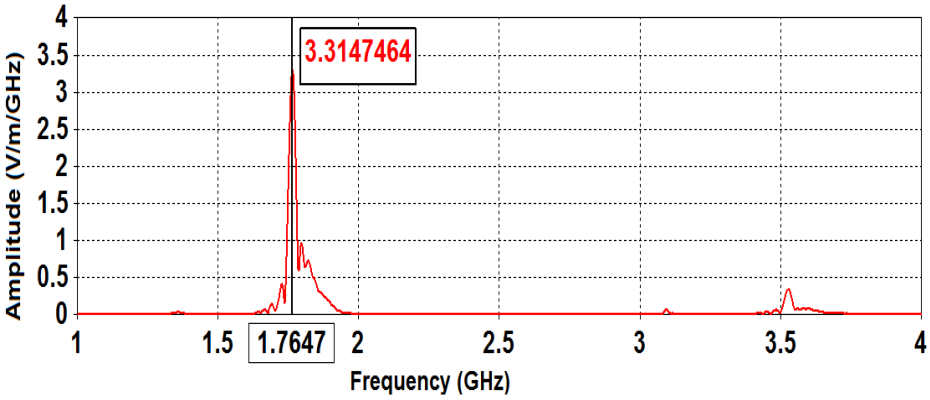

Figure 3.9: Frequency Spectrum at TM_{01} mode.

For beam-wave interaction process to takes place, first step is pre-oscillation phase at which magnetically insulated sheath is formed between tip of disc and cathode, at a specific current known as critical current. Amount of critical or charging current developed is shown in Figure 3.10. Spoke or RF current developed is shown in Figure 3.11.

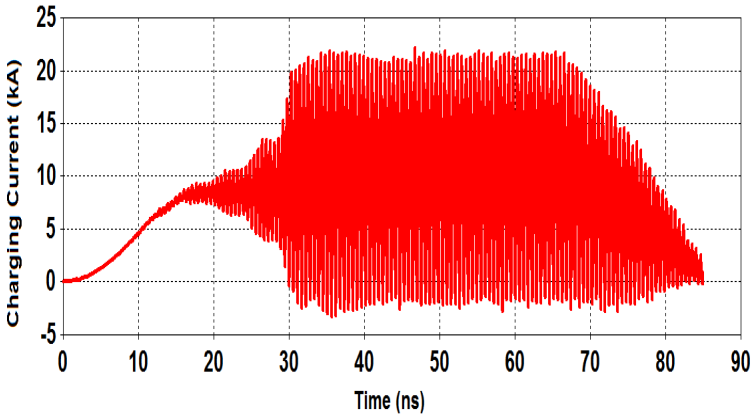

Figure 3.10: Charging or critical current for magnetic insulation.

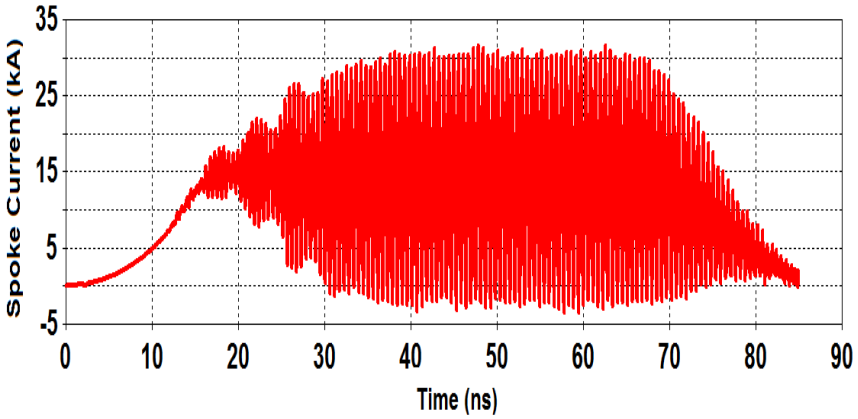

Figure 3.11: RF current developed during beam-wave interaction.

As explained in previous chapter, anode current is the sum of charging current and spoke current. Thus, anode or beam current developed is shown in Figure 3.12.

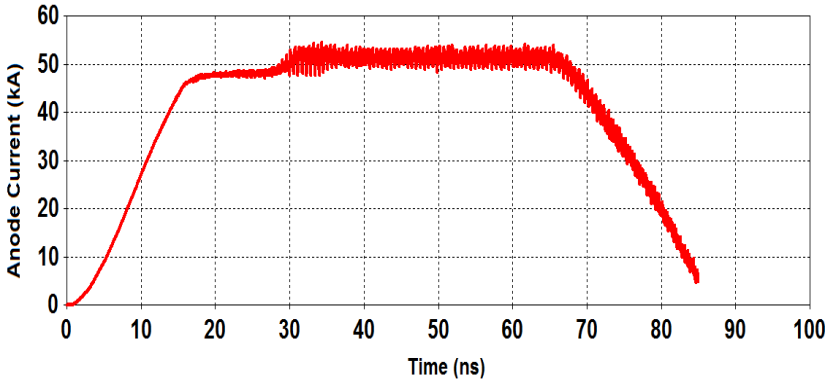

Figure 3.12: Beam Current developed during RF generation.

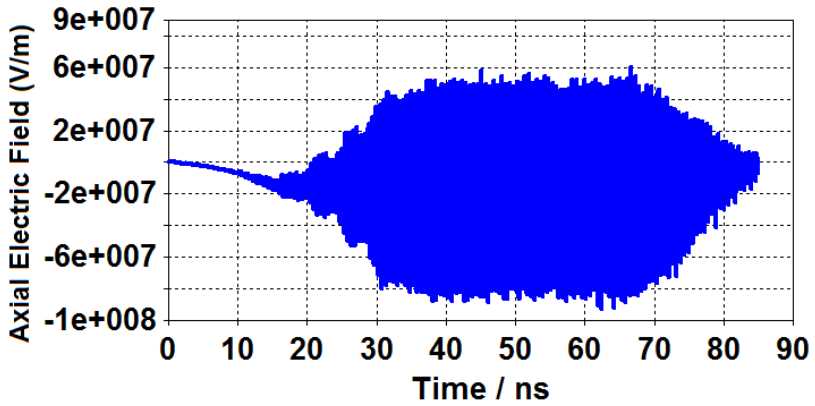

Figure 3.13: Temporal electric field amplitude for TM_{01} mode.

A probe is placed inside the interaction cavity at the position of maximum electric field and its signal is recorded in time domain shown in Figure 3.13. Electric field probe amplitude that have been obtained through simulation confirm the operation in the designed mode. The maximum of field has been observed across tip of disc and cathode along insulated sheath, which is essential for the maximum energy transfer during the beam-wave interaction. This electric field developed is responsible for space charge wave oscillations that induce RF inside the cavities. Expression for this electric field is derived in chapter 2.

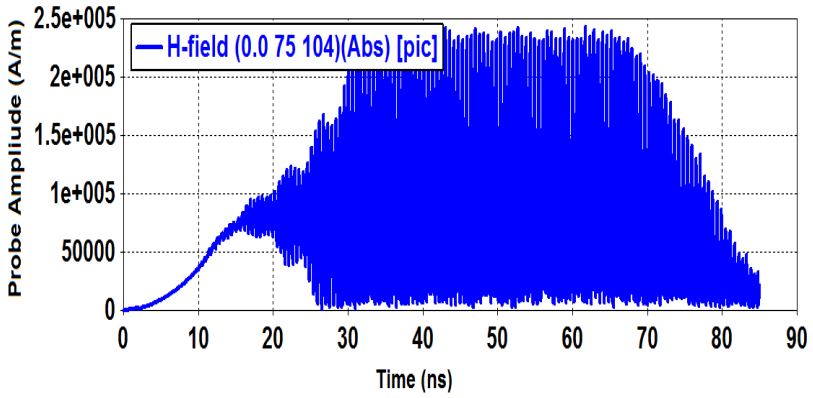

Figure 3.14: Self magnetic field amplitude developed for TM_{01} mode

Magnetic field probe amplitude that have been obtained through simulation confirm the generation of self magnetic field shown from Figure 3.14, that grazes the electrons from the anode surface and helps in confining the electrons between tip of discs and cathode.The energy distribution of all the particles along the interaction length has been shown in Figure 3.15. After magnetic insulation as electrons traverse forward along slow wave structure, beam-wave interaction takes place due to induced RF field across the interaction cavities. This field is generated when RF voltage is more than the DC beam voltage and it can be seen from Figure 3.15.

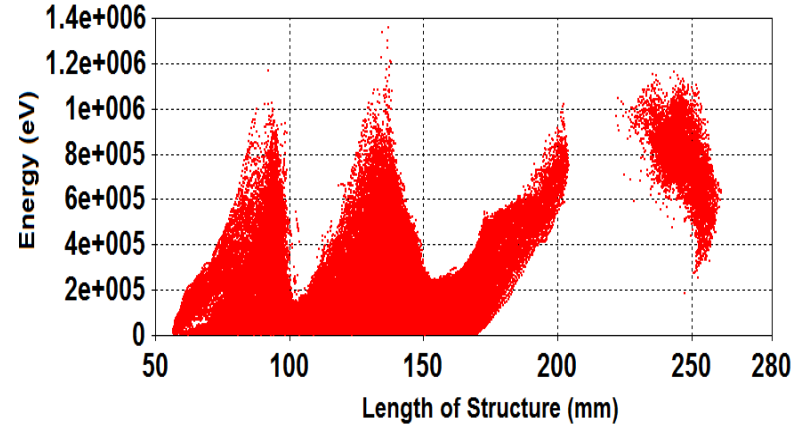

(a)

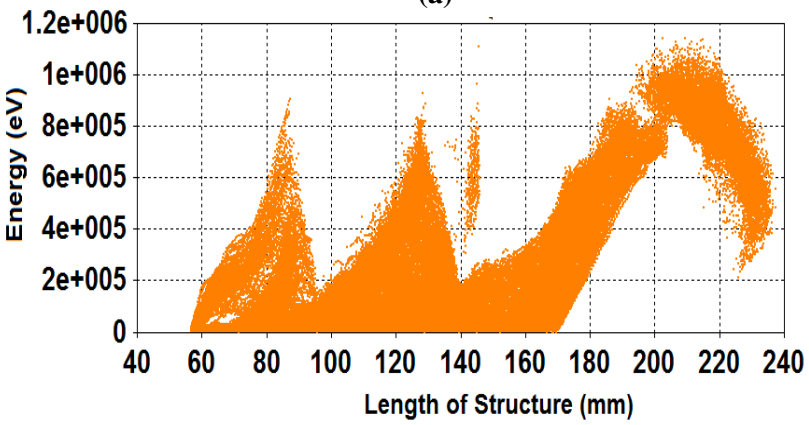

(b)

Figure 3.15: (a) Snapshot of bunching mechanisms, **(b)** energy transfer mechanism along interaction length.

When synchronisms condition occur, beam transfer its energy to RF in the form of spokes along the interaction length as shown from Figures 3.15a and b. While crossing the anode cathode gap spoke electron must acquire kinetic energy greater than or equal to the gap voltage shown nicely from Figures. Due to presence of RF voltage, field electrons experience simultaneous deceleration or acceleration while crossing the gap. From Figures, it has been visualized that electron beam velocity is decelerated in the RF interaction structure and this reduction of the kinetic energy is transferred to the RF field, this condition is necessary for proper beam-wave interaction in MILO which confirms that slow space charge waves are synchronized

with the electron beam. Figure 3.16, represents effect of repetitive pulse on device operation. It has been shown from Figure, till 30 ns rise time the electron flow is properly magnetically insulated and RF signal amplitude remain saturates for duration of pulse 20 ns till end of pulse. During repetitive pulse operation no significant pulse shortening is observed from for the defined pulse duration and this is only due to addition of quarter wavelength stubs during designing.

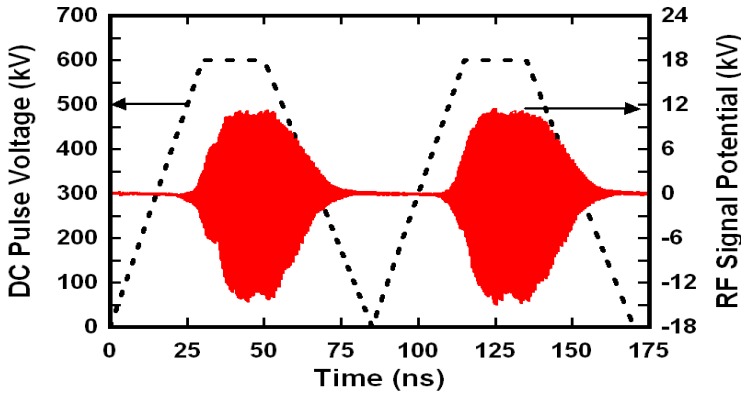

Figure 3.16: Effect of repetitive pulse on device operation.

For the proposed MILO conversion/electronic efficiency at TEM mode is 24% calculated using Equation (3.13) and the total efficiency for $P_{d.c}$= 31.2 GW and $P_{RF,out}$= 4.5 GW, is 14.4%.The PIC simulation results obtained here are in agreement with the reported experimental results within ~5%. Overall efficiency at TM_{01} mode is 19.2%.

3.5 Conclusion

A practical efficient HPM source, which does not required external DC magnetic field, compact MILO device is selected here for investigation of its beam wave interaction behaviour through 3D CST-PIC simulation. The basic device operating mechnism has been explained, describing MILO different sub-assembilies and its specific role in the device operation. Starting from the fundamentals, design methodology has been described properly taking into account impedances at input and

output end which is not explained yet,in conjunction with design of beam dump disk and position of stub to appreciate the device phyics.

In the present work, a commercial 3D PIC code 'CST-Particle Studio' has been configured for the MILO device to investigate the device beam wave interaction mehanisms considering various phase of oscillations. This gives information of temporal growth of RF signals of almost all frequencies in the RF output of MILO. At the different time intervals during simulation, the bunching process, electron spoke formation, magnetic insulation and energy transfer to the RF field along interaction length of the RF interaction structure of the device have been observed. The RF output power obtained by our simulation matches with those reported in the literature, which proves the validity of our simulation. During simulation peak power conversion efficiency is found to be 14.4%. The results shows that proposed MILO produces an RF output power ~ 4.5 GW for frequency of 1.76 GHz at TEM mode and 6 GW at TM_{01} mode. This become possible when two stubs or conducting rods are considered at output coaxial transmission line.

It is hoped that the present study and this paper would not be only useful to understand the basic device operation, electron beam and RF wave interaction mechanism in practical MILO device but also help the researcher working in this area for 3D PIC simulation of the device using commercial codes. Further, the simulation studies of MILO described in this chapter will be used in the subsequents chapters of this thesis to validate our developed analytical results.